

Unsupervised classification of acoustic emissions from catalogs and fault time-to-failure prediction

Hope Jasperson*, Chas Bolton, Paul Johnson, Chris Marone, Maarten V. de Hoop

Abstract

When a rock is subjected to stress it deforms by creep mechanisms that include formation and slip on small-scale internal cracks. Intragranular cracks and slip along grain contacts release energy as elastic waves called acoustic emissions (AE). Early research into AEs envisioned that these signals could be used in the future to predict rock falls, mine collapse, or even earthquakes. Today, nondestructive testing, a field of engineering, involves monitoring the spatio-temporal evolution of AEs with the goal of predicting time-to-failure for manufacturing tools and infrastructure. The monitoring process involves clustering AEs by damage mechanism (e.g. matrix cracking, delamination) to track changes within the material. In this study, we aim to adapt aspects of this process to the task of generalized earthquake prediction. Our data are generated in a laboratory setting using a biaxial shearing device and a granular fault gouge that mimics the conditions around tectonic faults. In particular, we analyze the temporal evolution of AEs generated throughout several hundred laboratory earthquake cycles. We use a Conscience Self-Organizing Map (CSOM) to perform topologically ordered vector quantization based on waveform properties. The resulting map is used to interactively cluster AEs according to damage mechanism. Finally, we use an event-based LSTM network to test the predictive power of each cluster. By tracking cumulative waveform features over the seismic cycle, the network is able to forecast the time-to-failure of the fault.

1 Introduction

Our motivation for this study comes from a field of engineering called nondestructive testing (NDT). The goal of NDT is to continuously assess the health of a material without removing it from operation or dismantling it in any way. NDT has many practical applications. In manufacturing, it is vital to identify when machine parts need to be repaired or replaced. In the realm of public safety, NDT can predict infrastructure collapse and prevent tragedy. NDT is commonly used in engineering and has been successfully applied to a wide range of materials, such as reinforced concrete [3], manufacturing tools [35], composite materials [17], and wood [9].

The NDT process begins by continuously recording acoustic data as the material of interest is in operation. For example, in [35], an acoustic sensor was affixed to the side of a cutting tool used in micro-machining in order to capture the acoustic signals produced. Acoustic data is gathered until the material reaches failure. In the lab, the failure process can be sped up by artificially subjecting the material to stress (e.g. [3, 7, 9, 13, 17]). Once the material has reached failure, the next step is to isolate the acoustic emissions within the acoustic data. An acoustic emission (AE) is a small elastic wave that is produced by the formation of small-scale internal cracks and slip along grain contacts. Thus, AEs provide a record of how the material internally responds to stress. Next, AEs are clustered according to mechanism using an unsupervised clustering algorithm. This step groups AEs according to the type of crack or deformation by which they were produced. In some studies, transmitted light (e.g. [17]) or scanning electron microscopy (e.g. [10]) is used to determine the true labels for each cluster. Finally, AE production throughout the failure cycle is analyzed in order to identify temporal patterns. In subsequent studies of the same material, these temporal patterns can be used to continuously predict time-to-failure.

In this study, our goal is to replicate the NDT process using laboratory-generated seismic data. Though the earthquake rupture process is somewhat different from the material failure studied in NDT, the underlying

*haj2@rice.edu

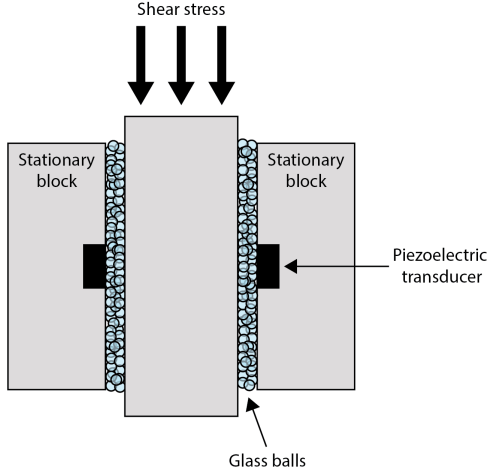


Figure 1: Schematic of the biaxial shearing system used to create the dataset.

physics of AE production are thought to be the same (e.g. [28, 18]). A previous study [26] used a similar laboratory dataset to predict time-to-failure, which suggests that the seismic signal contains predictive information. Here, we seek to identify the components of the seismic signal that carry predictive information in an effort to move towards a more generalized method of earthquake prediction.

2 Data description

The laboratory dataset was created using a biaxial shearing system that has been described in detail in previous work [14, 24, 26, 25]. Briefly, the system consists of a central block flanked on two sides by stationary blocks containing piezoelectric transducers that record acoustic signals, as in Figure 1. The stationary blocks are separated from the central block by a fault gouge consisting of glass beads that mimic real-Earth conditions. A piston applies shear stress to the central block, which drives it downwards, producing stick-slip events.

In this study, we use acoustic data from two laboratory experiments for a total of 350 stick-slip events. These events take place under a variety of stress conditions with shear stresses ranging from roughly 1 to 3.5 MPa. The time window from the beginning of stress application to the rupture (i.e. the failure cycle) averages around 10 seconds. Figure 2b is a snapshot of the acoustic data with AEs denoted by red circles. AEs were detected by the same process described in [19], though an unsupervised method like that of [29] could also be used. The two datasets combined contain about 8 million AEs and each failure cycle consists of several thousand AEs.

3 Damage mechanism clustering

3.1 Data processing

For the AE clustering, we use a set of five features typically used in NDT studies. Through experimentation, NDT researchers have determined that these five features are sufficient for AE clustering. The features are maximum amplitude, counts, duration, energy, and rise time (Figure 3). Counts is the number of positive peaks over the duration of the AE and rise time is the length of time until the maximum amplitude is reached. In addition, we use two frequency features, average frequency and peak frequency, which brings the total number of features to seven. In order to calculate features such as energy, the start and end times of the AEs must be known. Start and end times were determined using an amplitude threshold as described in [11]. During the processing procedure, we found that a simple 10% threshold was inadequate due to the large spread of maximum amplitudes. As a result, we used a decreasing threshold scheme whereby

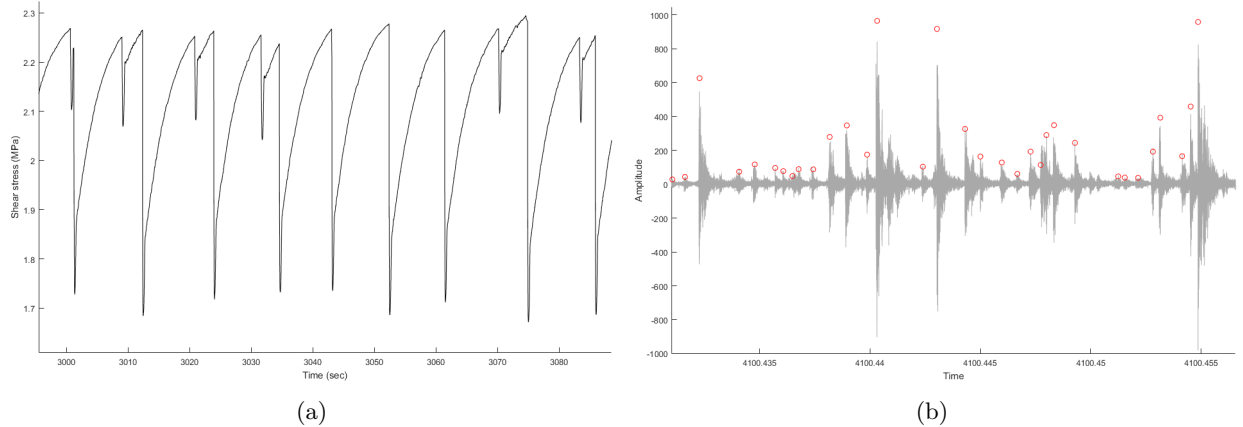


Figure 2: A) Shear stress. B) Snapshot of the acoustic data. Red circles are AEs.

the percentage used is decreased as the maximum amplitude increases. For very low amplitude events, the minimum amplitude is fixed to be slightly above the noise level. Despite these adjustments, amplitude thresholding is an imprecise tool, which may warrant further improvements in the future.

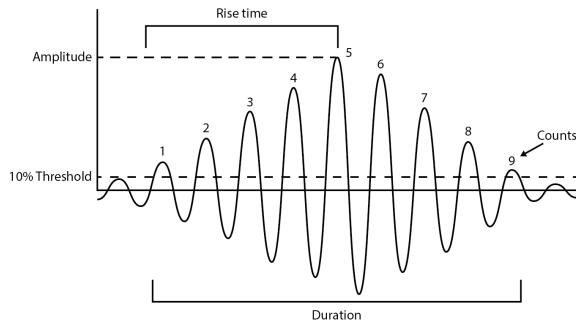


Figure 3: Four of the AE features used for classification

Unlike many NDT studies, we are not able to determine the true mechanism labels for the AEs. Though this means we will not be able to provide a full account of changes occurring in the fault gouge, labels are not required for our purposes. Our main goal is to identify elements of the acoustic signal that contain predictive information, which does not necessitate knowledge of the true labels.

3.2 Clustering procedure

For the AE clustering we use a conscience self-organizing map (CSOM) [8] which is a more efficient variant of the original Kohonen self-organizing map (KSOM) [16]. The CSOM was trained using a 15x15 lattice on over 8 million AEs for 20 million learning steps. Once training was complete, we used k-means and interactive interpretation to partition the CSOM lattice into clusters. We evaluated many potential cluster configurations using cluster validity indices (CVIs) including CH-VRC [4], Conn_Index [30], DBI [6], the Gap statistic [32], GDI [2], PBM [21], and Silhouette [15] and visualizations such as the U-matrix (and modified U-matrix), octagonal erosion, and CONNvis [33, 20, 5, 31]. Ultimately we found that an interactive clustering with a k value of 5 produced the best results. The trained and interpreted CSOM lattice is shown in Figure 4 along with the typical waveforms for each cluster. Note that since we do not have the true labels of these clusters, they will henceforth be referred to by color.

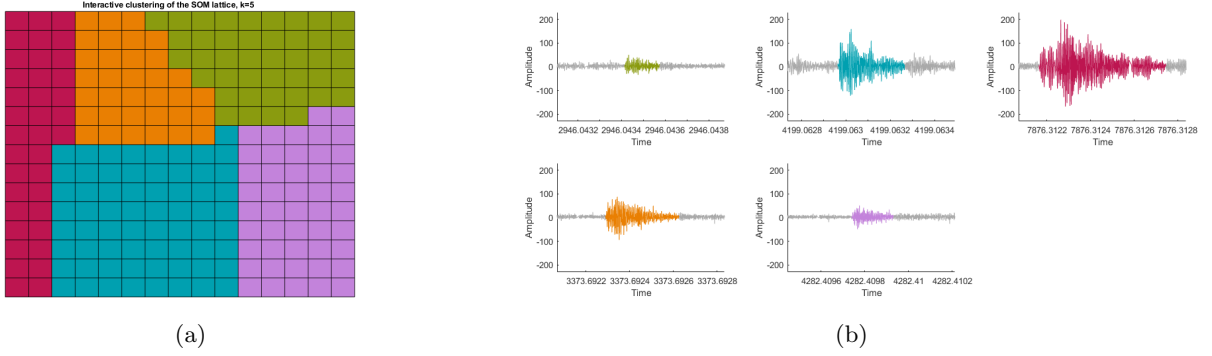


Figure 4: A) Trained SOM lattice. B) Typical waveforms for each of the five clusters.

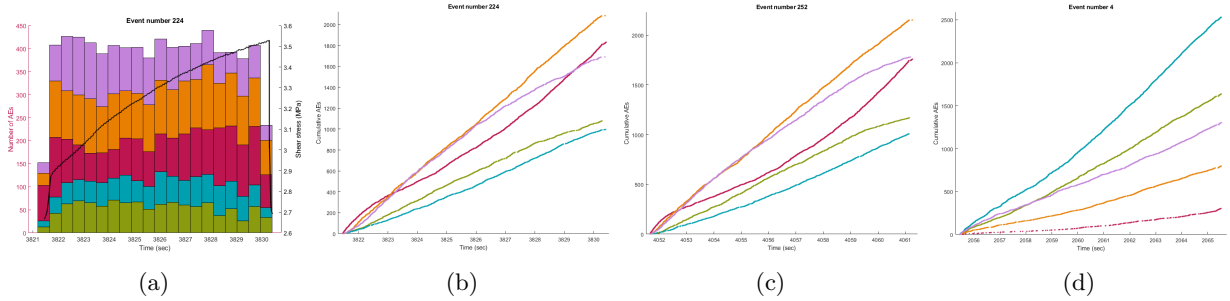


Figure 5: A) (Left axis) Histogram of the number of AEs by cluster. (Right axis) Shear stress. B-C) Cumulative AEs by cluster for two events of similar high stress. C) Cumulative AEs for a low stress event.

3.3 Results

We examined the production of AEs by cluster throughout the failure cycle. As is typically done in NDT studies, we plotted the cumulative number of AEs over the failure cycle (Figures 5a and 5b). These results resemble those obtained in NDT studies, which supports the notion that the process of AE production is similar in both instances. Most of the clusters display nonlinear behavior that may be useful for determining the percentage of the failure cycle that has elapsed. However, not all clusters appear to have predictive capability; the orange cluster is nearly linear and thus will not be useful for failure prediction.

Our results suggest that AE production is tied to the shear stress of the system. We observe that stick-slip events with comparable shear stress exhibit very similar cumulative AE patterns, as in Figures 5b and 5c. The similarity of these patterns indicates that AE production is not random and instead is indicative of some underlying phenomena. Though NDT studies frequently assume that failure events that occur under comparable stress conditions produce similar temporal AE patterns, little work has been done on the subject. In addition, we find that events at different stress levels produce different temporal patterns of AEs (Figures 5b and 5c vs. Figure 5d). This relationship effectively eliminates the possibility of time-to-failure prediction based exclusively on temporal patterns of AE production because the stress state of the fault is generally not known in the real Earth.

Recent work suggests an alternative feature for prediction. In [26], researchers predicted time-to-failure on a similar laboratory dataset using a sliding window on the raw acoustic data. They found that the variance of the signal was the most important feature for failure prediction. In this study, we focus exclusively on the AEs and thus it would be inappropriate to calculate continuous variance. However, when training the CSOM, we used AE energy as an input feature, which is related to variance. Figure 6a is a plot of the cumulative energy from all AEs for a single stick-slip event. As the system progresses towards failure, the amount of energy contained in the AEs increases according to a power law. This result suggests that the AEs contain the necessary information for time-to-failure prediction. Thus, prediction may be possible by monitoring cumulative waveform characteristics of the AEs and disregarding the rest of the acoustic signal.

To investigate the predictive capability of each AE type, we divide the cumulative energy by AE cluster,

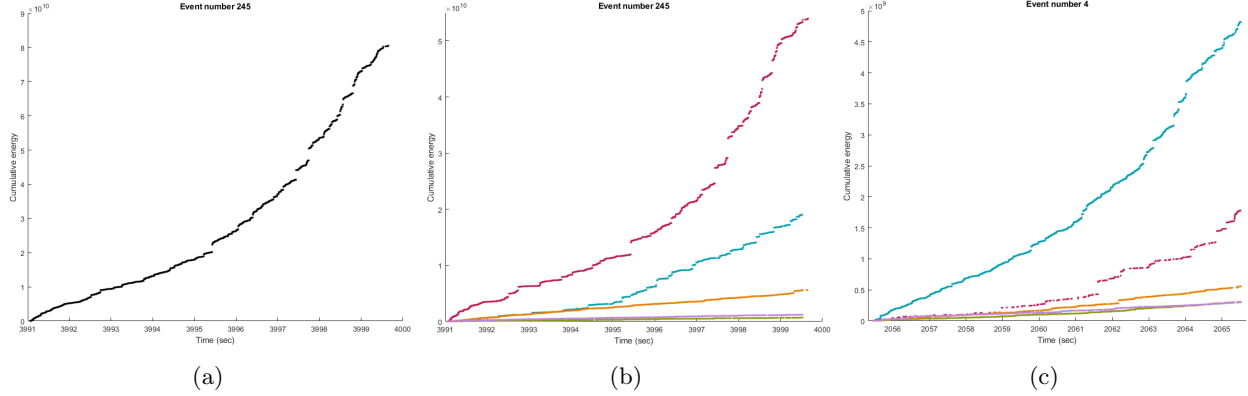


Figure 6: A) Cumulative energy for a single stick-slip event. B) Cumulative energy by cluster for a high stress event. C) Cumulative energy by cluster for a low stress event.

as in Figure 6b. At first glance, it appears that the red cluster is all that is needed for failure prediction because it contains the vast majority of the total AE energy. However, as with cumulative AEs, the stress state of the fault plays a role in the energy contained within in each cluster. Figure 6c shows the cumulative energy by cluster for a low stress event. Compared to the high stress event in Figure 6b, the proportion of the total energy contained in the red cluster is reduced. As a result, the blue cluster contains a much larger proportion of the total energy. This indicates that the blue cluster is a vital source of predictive information at low shear stress. The three remaining clusters contain very little energy and have linear trends, which indicates that they will not be useful for prediction. These findings suggest that we can predict time-to-failure at all relevant stress levels using only information from the red and blue AE clusters.

4 Time-to-failure prediction

4.1 Data processing and network configuration

For time-to-failure prediction, we only use AEs from the red and blue clusters. There are three reasons for this. First, as discussed in the previous section, the remaining three clusters are not expected to contain predictive information. Second, our experiments show that training on a single cluster is less accurate than training on both the red and blue clusters. Finally, training the network on two clusters is substantially faster than training on all five. Due to uneven cluster sizes, training on the full dataset takes over five times as long as training on only these two clusters. In addition, training on all five clusters did not improve prediction error. Network inputs consist of the seven features used to train the CSOM as well as cumulative number of AEs. All eight input features are cumulative by cluster. Though using cumulative energy as the only input feature produced good results, we found that using all eight features yielded slight gains. All input features were normalized to $[0,1]$ according to their maximum and minimum values across the entire dataset.

In order to maintain the temporal ordering of AEs while considering multiple clusters, each input contains all eight features for each relevant cluster. Thus, for two clusters the input size is 16. Each input contains the features for the current AE as well as the features for the previous AE from every other cluster. Over time, the inputs resemble a step function where the features for each cluster are held constant until an AE from that cluster occurs.

To further improve results, we apply a technique from engineering that is commonly used in remaining useful life (RUL) predictions for machinery. Many studies have successfully forecasted RUL using recurrent networks on continuous mechanical data gathered while the equipment is in operation [22, 23, 34, 36, 37]. [12] first suggested replacing the actual RUL with a piecewise function where RUL is initially set to some constant value. Once this value is reached, RUL decreases as usual. The reasoning is that RUL is very hard to predict early in the failure cycle when the material is healthy. Several studies have since shown that using a piecewise RUL reduces prediction error (e.g. [34, 37]). Here we apply this same concept to fault

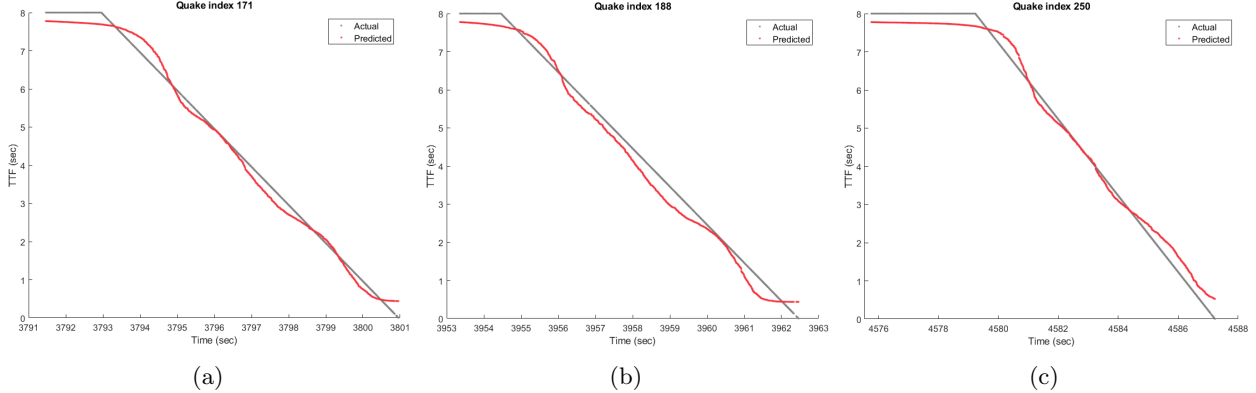


Figure 7: Actual vs. predicted time-to-failure for three events.

time-to-failure prediction. We used an initial constant value of 8 seconds which led to a substantial decrease in both train and test error.

We predicted time-to-failure using a vanilla LSTM network with 5 layers and a hidden size of 1. The network was trained using the Adam optimizer and an adaptive learning rate. The training set consisted of 284 randomly selected stick-slip events and the test set contained the remaining 70 events. The network predicted time-to-failure at each AE and calculated error using smooth L1 loss. We used a batch size of 50 AEs and trained for 150 epochs.

4.2 Results

Figure 9 shows the actual and predicted time-to-failure for three events as well as a heatmap for all AEs. The smooth L1 loss is 0.64 for the full training set and 0.85 for the full test set, though most test events have lower individual losses (see section 5). These results show that the network is able to learn the structure of the cumulative AE features and use it to make reasonably accurate predictions of time-to-failure throughout the earthquake cycle.

5 Discussion and conclusion

We identified a few areas where our method could be improved. First, the network architecture should be modified to address the irregular time steps between AEs. LSTM networks assume that the input data is regularly sampled and thus that the time steps between data points are uniform across the entire dataset. However, the AE data is event-based so distance in time between adjacent AEs varies, as in Figure 8a. A number of networks (e.g. [1, 27, 38]) have been proposed in the last few years that scale network parameters according to the time elapsed between input points (Figure 8b). Using a similar network for the AE data would likely lead to decreased prediction error.

Time-to-failure predictions could also be improved by using a more balanced dataset. The majority of events have a cycle length around 10 seconds, but some are significantly longer or shorter (Figure 9a). Since these very long/short events are underrepresented in the dataset, they generally have high prediction error, as in Figure 9b. The prediction error is especially high if the random draw places most of these events in the test set. In order to improve accuracy, more of these very long/short events should be added to the dataset.

In this study, we adapted health monitoring approaches from engineering to predict time-to-failure for laboratory generated earthquakes. Our experiments successfully predicted time-to-failure using a novel method that combined AE clustering from NDT with failure forecasting techniques from RUL prediction. This study shows that the overall method is a promising approach to generalized earthquake prediction.

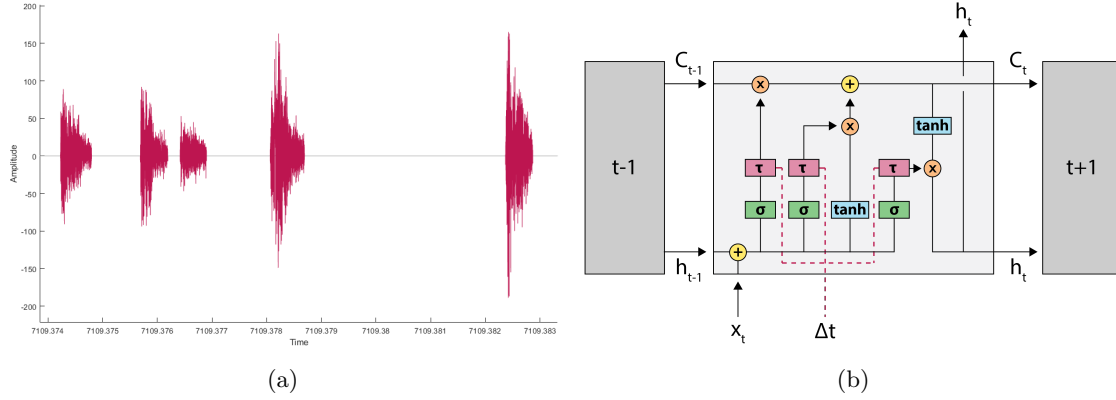


Figure 8: A) Data snapshot showing irregular time steps between AEs. B) LSTM cell from the Time-Gated LSTM model proposed in [27]. The network input includes the distance in time between data points and scales the gate outputs accordingly.

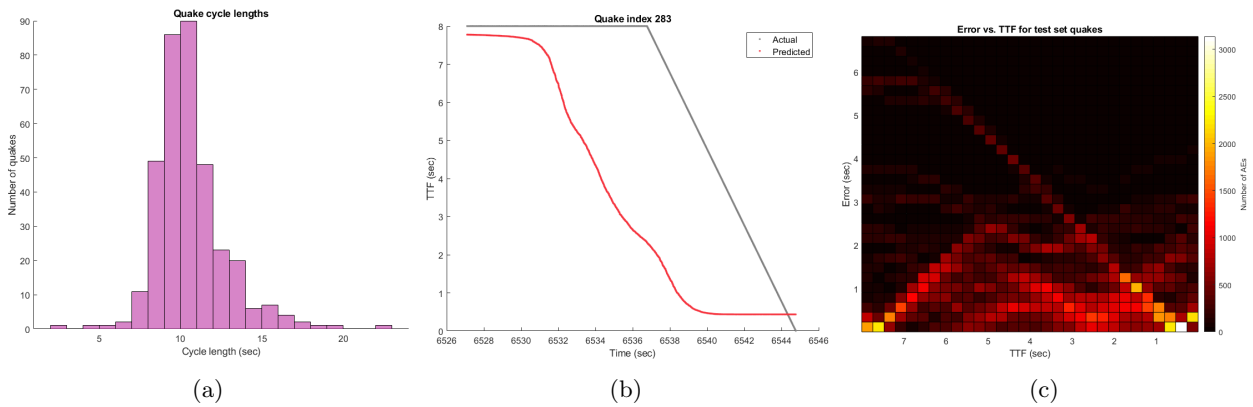


Figure 9: A) Distribution of failure cycle lengths. B) Time-to-failure predictions for an event with an unusually long failure cycle. C) Heatmap of error (in sec) over time for all AEs in all test set events. The line of high error corresponds to underrepresented events.

6 Acknowledgments

This work was supported by the U.S. Department of Energy under grant number DE-SC0020345. Special thanks to Erzsebet Merenyi for the use of the NeuroScope software tools for CSOM training.

References

- [1] I. M. BAYTAS, C. XIAO, X. ZHANG, F. WANG, A. K. JAIN, AND J. ZHOU, *Patient subtyping via time-aware LSTM networks*, in Proceedings of the 23rd ACM SIGKDD International Conference on Knowledge Discovery and Data Mining, KDD '17, ACM, 2017, pp. 65–74.
- [2] J. C. BEZDEK AND N. R. PAL, *Some new indexes of cluster validity*, IEEE Transactions on Systems, Man, and Cybernetics, Part B (Cybernetics), 28 (1998), pp. 301–315.
- [3] L. CALABRESE, G. CAMPANELLA, AND E. PROVERBIO, *Identification of corrosion mechanisms by univariate and multivariate statistical analysis during long term acoustic emission monitoring on a pre-stressed concrete beam*, Corrosion Science, 73 (2013), pp. 161 – 171.
- [4] T. CALISKI AND J. HARABASZ, *A dendrite method for cluster analysis*, Communications in Statistics, 3 (1974), pp. 1–27.
- [5] M. COTTRELL AND E. DE BODT, *A kohonen map representation to avoid misleading interpretations*, in Proc. 4th European Symposium on Artificial Neural Networks, 1996, pp. 103–110.
- [6] D. L. DAVIES AND D. W. BOULDIN, *A cluster separation measure*, IEEE Transactions on Pattern Analysis and Machine Intelligence, PAMI-1 (1979), pp. 224–227.
- [7] R. DE OLIVEIRA AND A. MARQUES, *Health monitoring of FRP using acoustic emission and artificial neural networks*, Computers & Structures, 86 (2008), pp. 367 – 373. Smart Structures.
- [8] D. DESIENO, *Adding a conscience to competitive learning*, in IEEE 1988 International Conference on Neural Networks, vol. 1, 1988, pp. 117–124.
- [9] M. DIAKHATE, E. BASTIDAS-ARTEAGA, R. M. PITTI, AND F. SCHOEFS, *Cluster analysis of acoustic emission activity within wood material: Towards a real-time monitoring of crack tip propagation*, Engineering Fracture Mechanics, 180 (2017), pp. 254 – 267.
- [10] N. FALLAHI, G. NARDONI, R. PALAZZETTI, AND A. ZUCHELLI, *Pattern recognition of acoustic emission signal during the mode I fracture mechanisms in carbon-epoxy composite*, in 32nd European Conference on Acoustic Emission Testing 2016, 2016, pp. 415–421.
- [11] N. GODIN, S. HUGUET, R. GAERTNER, AND L. SALMON, *Clustering of acoustic emission signals collected during tensile tests on unidirectional glass/polyester composite using supervised and unsupervised classifiers*, NDT & E International, 37 (2004), pp. 253 – 264.
- [12] F. O. HEIMES, *Recurrent neural networks for remaining useful life estimation*, in 2008 International Conference on Prognostics and Health Management, Oct 2008, pp. 1–6.
- [13] S. HUGUET, N. GODIN, R. GAERTNER, L. SALMON, AND D. VILLARD, *Use of acoustic emission to identify damage modes in glass fibre reinforced polyester*, Composites Science and Technology, 62 (2002), pp. 1433–1444.
- [14] P. A. JOHNSON, B. FERDOWSI, B. M. KAPROTH, M. SCUDERI, M. GRIFFA, J. CARMELIET, R. A. GUYER, P. L. BAS, D. T. TRUGMAN, AND C. MARONE, *Acoustic emission and microslip precursors to stickslip failure in sheared granular material*, Geophysical Research Letters, 40 (2013), pp. 5627–5631.
- [15] L. KAUFMAN AND P. ROUSSEEUW, *Finding groups in data: An introduction to cluster analysis*, 1990.
- [16] T. KOHONEN, *Self-organized formation of topologically correct feature maps*, Biological Cybernetics, 43 (1982), pp. 59–69.
- [17] L. LI, S. V. LOMOV, AND X. YAN, *Correlation of acoustic emission with optically observed damage in a glass/epoxy woven laminate under tensile loading*, Composite Structures, 123 (2015), pp. 45 – 53.
- [18] D. LOCKNER AND J. BYERLEE, *Acoustic emission and creep in rock at high confining pressure and differential stress*, Bulletin of the Seismological Society of America, 67 (1977), p. 247258.

- [19] N. LUBBERS, D. C. BOLTON, J. MOHD-YUSOF, C. MARONE, K. BARROS, AND P. A. JOHNSON, *Earthquake catalog-based machine learning identification of laboratory fault states and the effects of magnitude of completeness*, *Geophysical Research Letters*, 45 (2018), pp. 13,269–13,276.
- [20] E. MERNYI, A. JAIN, AND T. VILLMANN, *Explicit magnification control of self-organizing maps for forbidden data*, *IEEE Trans. Neural Networks*, 18 (2007), pp. 786–797.
- [21] M. K. PAKHIRA, S. BANDYOPADHYAY, AND U. MAULIK, *Validity index for crisp and fuzzy clusters*, *Pattern Recognition*, 37 (2004), pp. 487 – 501.
- [22] L. REN, J. CUI, Y. SUN, AND X. CHENG, *Multi-bearing remaining useful life collaborative prediction: A deep learning approach*, *Journal of Manufacturing Systems*, 43 (2017), pp. 248 – 256.
- [23] M. RIGAMONTI, P. BARALDI, E. ZIO, I. ROYCHOUHURY, K. GOEBEL, AND S. POLL, *Echo state network for the remaining useful life prediction of a turbofan engine*, in *European Conference of the Prognostics and Health Management Society*, 2016.
- [24] J. RIVIERE, Z. LV, P. JOHNSON, AND C. MARONE, *Evolution of b-value during the seismic cycle: Insights from laboratory experiments on simulated faults*, *Earth and Planetary Science Letters*, 482 (2018), pp. 407 – 413.
- [25] B. ROUETLEDUC, C. HULBERT, D. C. BOLTON, C. X. REN, J. RIVIERE, C. MARONE, R. A. GUYER, AND P. A. JOHNSON, *Estimating fault friction from seismic signals in the laboratory*, *Geophysical Research Letters*, 45 (2018), pp. 1321–1329.
- [26] B. ROUETLEDUC, C. HULBERT, N. LUBBERS, K. BARROS, C. J. HUMPHREYS, AND P. A. JOHNSON, *Machine learning predicts laboratory earthquakes*, *Geophysical Research Letters*, 44 (2017), pp. 9276–9282.
- [27] S. O. SAHIN AND S. S. KOZAT, *Nonuniformly sampled data processing using lstm networks*, *IEEE Transactions on Neural Networks and Learning Systems*, 30 (2018), pp. 1452–1461.
- [28] C. H. SCHOLZ, *Microfracturing and the inelastic deformation of rock in compression*, *Journal of Geophysical Research* (1896-1977), 73 (1968), pp. 1417–1432.
- [29] L. SEYDOUX, R. BALESTRIERO, P. POLI, M. V. DE HOOP, M. CAMPILLO, AND R. BARANIUK, *Accelerating seismicity before the 2017 Nuugaatsiaq landslide revealed from unsupervised deep learning*, 2019.
- [30] K. TASDEMIR AND E. MERENYI, *A validity index for prototype-based clustering of data sets with complex cluster structures*, *IEEE Transactions on Systems, Man, and Cybernetics, Part B (Cybernetics)*, 41 (2011), pp. 1039–1053.
- [31] K. TASDEMIR AND E. MERNYI, *Exploiting data topology in visualization and clustering of self-organizing maps*, *IEEE Trans. Neural Networks*, 20 (2009), pp. 549–562.
- [32] R. TIBSHIRANI, G. WALTHER, AND T. HASTIE, *Estimating the number of clusters in a data set via the gap statistic*, *Journal of the Royal Statistical Society: Series B (Statistical Methodology)*, 63 (2001), pp. 411–423.
- [33] A. ULTSCH AND H. SIEMON, *Kohonen’s self organizing feature maps for exploratory data analysis*, in *Proc. of the International Neural Network Conference*, 1990, p. 305308.
- [34] Y. WU, M. YUAN, S. DONG, L. LIN, AND Y. LIU, *Remaining useful life estimation of engineered systems using vanilla lstm neural networks*, *Neurocomputing*, 275 (2018), pp. 167 – 179.
- [35] C.-L. YEN, M.-C. LU, AND J.-L. CHEN, *Applying the self-organization feature map (SOM) algorithm to AE-based tool wear monitoring in micro-cutting*, *Mechanical Systems and Signal Processing*, 34 (2013), pp. 353–366.

- [36] A. S. YOON, T. LEE, Y. LIM, D. JUNG, P. KANG, D. KIM, K. PARK, AND Y. CHOI, *Semi-supervised learning with deep generative models for asset failure prediction*, 2017.
- [37] S. ZHENG, K. RISTOVSKI, A. FARAHAT, AND C. GUPTA, *Long short-term memory network for remaining useful life estimation*, in 2017 IEEE International Conference on Prognostics and Health Management (ICPHM), June 2017, pp. 88–95.
- [38] Y. ZHU, H. LI, Y. LIAO, B. WANG, Z. GUAN, H. LIU, AND D. CAI, *What to do next: Modeling user behaviors by time- lstm*, in Proceedings of the 26th International Joint Conference on Artificial Intelligence, IJCAI'17, AAAI Press, 2017, pp. 3602–3608.